


Article

# Axial Flux Permanent Magnet Synchronous Generators for Pico Hydropower Application: A Parametrical Study

Vincenzo Di Dio \*, Giovanni Cipriani  and Donatella Manno 

Department of Engineering, University of Palermo, 90128 Palermo, Italy

\* Correspondence: vincenzo.didio@unipa.it; Tel.: +39-09123860299

**Abstract:** A pico hydropower plant is an energy harvesting system that allows energy production using the power of the water flowing in small watercourses, and in water distribution network. Axial Flow Flux Permanent Magnet Synchronous Generator (AFPMSG) are particularly suitable for this application, being efficient machines that achieve high power with small dimensions. This paper presents a parametrical study of several configurations and topologies of three-phase and single-phase AFPMSG, for pico hydropower application, to assess the most suitable dimensional characteristics for the most energy production using a safe voltage of 25 V. The AFPMSGs here considered has a simple single stator and rotor configuration, commercial-type permanent magnets, and concentric windings, to facilitate their cost-effective construction and the spread of their use also in developing countries. For each AFPMSG considered, the power output was calculated using 3-D modelling and Finite Element Analysis; besides, the different parameters and features that affect the power output were evaluated at different rotational speeds. The results achieving a power density up to 100 W/cm<sup>3</sup>, at 1000 rpm with energy produced to 1.7 kWh/day.

**Keywords:** pico hydropower; energy harvesting; hydropower; axial flux permanent magnet; synchronous generator; hydro generator



**Citation:** Di Dio, V.; Cipriani, G.; Manno, D. Axial Flux Permanent Magnet Synchronous Generators for Pico Hydropower Application: A Parametrical Study. *Energies* **2022**, *15*, 6893. <https://doi.org/10.3390/en15196893>

Academic Editor: Frede Blaabjerg

Received: 26 July 2022

Accepted: 16 September 2022

Published: 21 September 2022

**Publisher's Note:** MDPI stays neutral with regard to jurisdictional claims in published maps and institutional affiliations.



**Copyright:** © 2022 by the authors. Licensee MDPI, Basel, Switzerland. This article is an open access article distributed under the terms and conditions of the Creative Commons Attribution (CC BY) license (<https://creativecommons.org/licenses/by/4.0/>).

## 1. Introduction

Hydropower is an important renewable resource used for the production of electricity [1], able to reduce greenhouse gas emissions [2]. In comparison to other renewable resources and fossil fuels, hydropower is a zero carbon footprint technology that uses a resource available in several parts of the globe, allowing applications in industrialized and remote areas [3].

The realization of high-power hydropower plants generally requires the creation of an artificial lake or invasive hydraulic structures causing significant environmental impacts [4], such as the habitat dispersion in aquatic and marine ecosystems, and socio-economic impacts. Moreover, climate change and the global temperature increase, in the last years, have caused a reduction in the flow rate of watercourses due to the evaporation process [5] which could compromise the energy production and limit the payback ratio and the profits of large hydropower plants. In the next years, climate change is forecast to reduce the profitability of large and small hydropower plants by 20% [6]. In 2019, the worldwide installed capacity amounted to 1308 GW with an annual production of 4306 TWh; according to data published by [7], installed capacity has increased of 1.2% in comparison to 2018.

In certain countries such as Italy, the use of resources of lesser water capacity is increasing due to the complete utilization of large watersheds or large rivers started several years ago. This trend is highlighted by the reduction in the average size of hydroelectric plants in service. Indeed, the average size of hydroelectric plants decreased from 8.2 MW in 2007 to 4.4 MW in 2018, and, considering only plants smaller than 1 MW, the average size increased from 0.37 MW in 2007 to 0.27 MW in 2018 [7,8]. During the same years, the

number of hydroelectric plants with a capacity under 1 MW increased from 1194 to 3123, up 162% while the number of larger hydropower plants with a capacity more than 10 MW increased by 5% [9,10].

A multitude of plant sizes is available for hydroelectric power generation. The European Commission classifies hydroelectric plants based on their rated power in large hydropower plants (with rated power greater than 10 MW) and small hydropower plants [1]. In the same way, small hydropower plants are categorized into mini hydropower plants up to 2 MW, micro hydropower plants below 500 kW, and pico hydropower plants less than 5 kW [11].

Pico hydropower plants can be realized through limited changes to existing water infrastructure. This allows to harvest energy in small watercourses, water waste treatment plants [12], and water distribution networks [13]. These systems can be connected to the grid [14] or used in stand-alone mode to supply local electrical loads, especially in remote areas. Specifically, some applications make it possible to power LEDs [15], small electrical loads [16,17] and laptop batteries [18] producing power from 114 W to 2 kW. Pico Hydropower plants can, also, be realized with cost-effective technologies [19], which present an annual life cycle cost from \$74/year to \$150/year to power a 200 W domestic load [20]. This price is competitive in comparison with the price for the production of energy from other renewable sources [21]. In recent years, technological innovations in the pico hydropower field have focused on the creation of low-cost and user-friendly systems to supply domestic load [22]. The constructive challenge is related to the miniaturisation of the electric generator and the choice of construction parameters to maximize the electrical energy produced under different operating conditions.

The generators normally used in hydroelectric plants are:

- Induction Generators (IG):
  - a. squirrel-cage IG;
  - b. doubly fed IG;
- Synchronous Generator (SG):
  - c. brushed SG: with Direct Current (DC) or static excitation;
  - d. brushless SG: with rotating diode bridge or Permanent Magnet (PM).

IG is commonly used for large hydropower, thanks to the low maintenance costs in the squirrel cage configuration. Doubly fed are commonly used for wind generation [23]. However, they have innovative applications in the large hydropower field, thanks to their many advantages, including the ability to generate power at variable speed and high water flow rates [24]. Brushed SG with Direct Current (DC) or static excitation brushed SG is used in large hydropower applications due to the low efficiencies for a size smaller than a few MW [25]. Brushless SG is designed using a rotating diode bridge excitation system or PM; these generators are very popular thanks to the low maintenance costs due to the lack of brushes. The PMGS with rare-earth PM is an efficient solution in small hydropower [26] compared to the use of ferrite, which leads to a decrease in generated torque, due to the residual flux density of about one-third [27]. PMGS can be realised in a radial configuration (cylindrical) [28] or an axial configuration (disc-type), called Axial Flux Permanent Magnet Synchronous Generator (AFPMSG) [29]. AFPMSGs are efficient machines that achieve high power with small dimensions [30]. Moreover, AFPMSGs are easily achievable and low-priced, and the largest part of its cost is due to the manufacture of Permanent Magnets (PM). Furthermore, AFPMSGs are designed for different rotational speeds in different papers, achieving high performance even [31] at 600 rpm, [17] 400 rpm and [32] at 859 rpm.

This paper presents a parametrical study of several configurations and topologies Axial Flux Permanent Magnet Synchronous Generators (AFPMSG), for pico hydropower application. It aims to find the most suitable dimensional characteristics of the AFPMSG, in particular the outer diameter, that allows the most energy production in a cost-effective manner. The three-phase and single-phase considered AFPMSGs topologies were designed

with simple-to-build, small size, and commercially available PM configurations to reduce the cost of manufacturing and further this technology accessible to developing country populations. Moreover, AFPMSGs proposed topologies were realized with a peak voltage value induced on the windings lower than the 25 V (safety voltage threshold), to design an intrinsically safe generator against electrocution, which can be employed in different applications without the requirement of additional safety systems. For each considered topology of AFPMSG, 3-D modelling and Finite Element Analysis (FEA) were performed to identifying the optimal setup of the different parameters and features which affect the power output. The magneto dynamic behavior and the flux density in the air-gap, the induced voltages on the stator windings, and the power generated by the no-load test and load test were evaluated for 48 configurations. These configurations were obtained by varying the air-gap thickness, the number of polar pairs, the PM size, the internal diameter value, the number of turns and slot fill factor value. The simulations also allow to evaluate the AFPMSG performances at different rotational speeds to assess the coupling between the proposed generator and a turbine. Furthermore, the configuration of the AFPMSG that achieved the best results was studied for a rotation speed range of 100 to 1000 rpm. The results show that AFPMSG for pico hydropower application into the small watercourse and water distribution network is an efficient solution for harvesting energy, allowing loads to be supplied in both stand-alone and grid-connected systems.

## 2. Mathematical Model of an Axial Flux Permanent Magnet Synchronous Generator for Pico Hydropower Application

A pico hydropower for stand-alone or grid-connected systems can be realised by coupling a turbine with an electric generator. The power produced by the pico hydropower system is fed into the grid or used to supply loads.

The rated voltage of a pico hydropower system is from 12 to 120 V in DC [33] or from 120 to 480 V in AC, with frequencies of variable value according to the speed of the turbine [34]. The connection of the plant to the power grid or to loads generally requires a step-up transformer to increase the voltage level [35]. To supply the loads, the system can be equipped with energy storage made up by a storage battery and by its power electronics systems [36]. The energy storage provides the loads when the hydropower system is not producing sufficient power. A Dump Load can be also connected to the stand-alone system for dissipating the excess electricity produced. A summary overview of the application is shown in Figure 1.

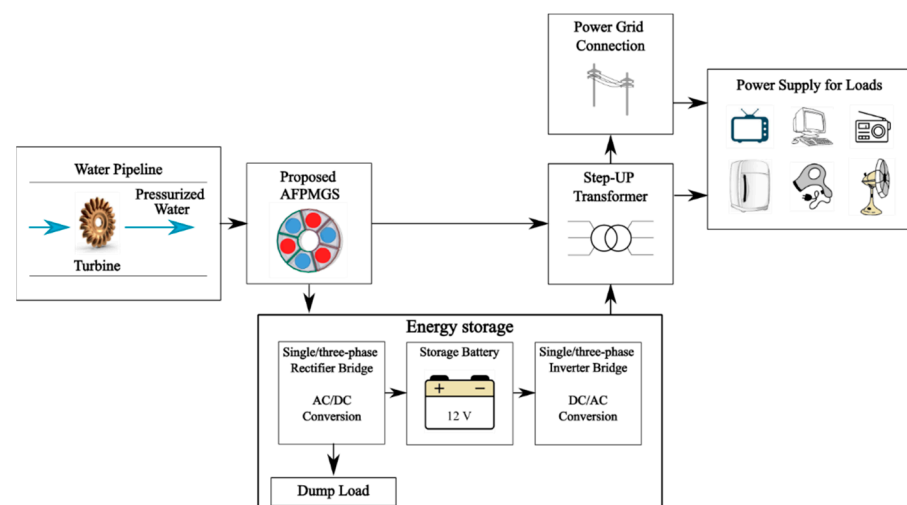


Figure 1. Overview for pico hydropower application.

For pico hydropower applications, it is possible to use impulse or reaction turbines or pump as turbines [37], according to the water flow and site head. The water flow can

be stored and subsequently conveyed in a pipeline or a penstock. This allows the varying the water flow rate and the head. The pico hydropower plant can also be realized in a run-of-river manner, using the water flow of a river [38].

In pico hydropower plants AFPMGS are commonly used, which can be realized with one or several rotors and stators, depending on the power output required for the application [39]. Moreover, for high turbine rotation speeds, it is also possible to realize AFPMGS with a high number of polar pairs. The AFPMGS can also be realized with or without stator slots (slotted or slotless) [40] and armature core (cored or coreless) [41], by installing PMs on the rotor surface or inside of the rotor and using a single-phase or a three-phase configuration. A single-phase generator is simpler and cost-effective to manufacture and maintenance, and can directly supply single-phase loads, while a three-phase generator is commonly used for industrial applications and can be connected directly to the power grid, but its maintenance cost is higher than that of a single-phase generator [42].

The sizing of the AFPMGS is generally carried out according to the output power ( $P_{out}$ ). In order to determine the power output of the generator, represented by Equation (11) assuming to neglect the resistance and loss inductance of the stator [38], it is necessary to take into account the quantities indicated in Table 1 and well known in the literature.

**Table 1.** Equations for calculating the generator output power.

Mathematical Equation	Equation Number	Reference
$P_{out} = \eta \frac{m}{T} \int_0^T e(t)i(t)dt = \eta m K_p E_{pk} I_{pk}$	(1)	[43]
$E_{pk} = K_e N_{ph} B_g \frac{f}{P_p} (1 - \lambda^2) D_0^2$	(2)	[39]
$I_{pk} = A \pi K_i \frac{1 + \lambda}{2} \frac{D_0}{2m_1 N_{ph}}$	(3)	[44]
$B_g = \frac{2l_3 \mu_0 B_r H_c}{B_{rg} + 2l_3 \mu_0 H_c}$	(4)	[45]
$K_e = \pi \sqrt{2} N K_w \phi_f$	(5)	[29]
$K_w = K_d K_p$	(6)	[46]
$K_d = \frac{\sin(\pi/m_1)}{q_1 \sin(\pi/2m_1 q_1)}$	(7)	[46]
$K_p = \cos\left(\frac{a}{2}\right)$	(8)	[46]
$K_p = \frac{1}{T} \int_0^T \frac{e(t)i(t)}{E_{pk} I_{pk}} dt$	(9)	[43]
$K_i = \frac{I_{pk}}{\sqrt{\frac{1}{T} \int_0^T \left(\frac{i(t)}{I_{pk}}\right)^2 dt}}$	(10)	[47]

The general-purpose sizing equation considered in this paper, allows to evaluate the  $P_{out}$  as a function of the AFPMGS construction parameters (rotor; stator; PM; windings) as shown in Equation (11) [48,49]. The procedure for determining the different constructional parameters of the AFPMGS according to the desired  $P_{out}$  is shown in Figure 2.

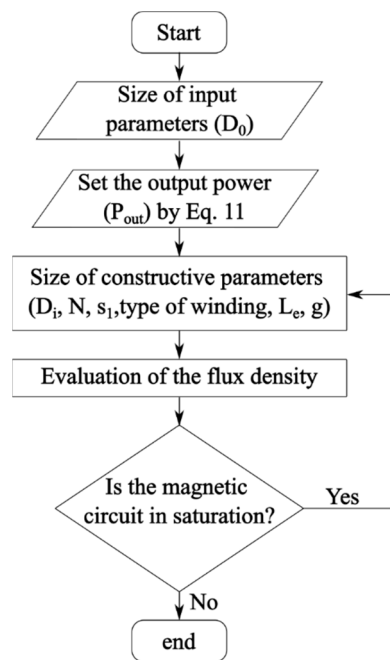


**Figure 2.** Choice of AFPMGS parameters and constructive characteristics.

$$P_{out} = \frac{1}{1 + K_{\phi}} \frac{m}{m_1} \frac{\pi}{2} K_e K_i K_p K_L \eta B_g A \frac{f}{p_p} (1 - \lambda^2) \left( \frac{1 + \lambda}{2} \right) D_0^2 L_e \quad (11)$$

The AFPMGS outer diameter  $D_0$  is set by the pico hydropower construction characteristics as the diameter of the coupled turbine [50]. The internal diameter ( $D_i$ ) of the generator can be selected using Equation (12) [43] from the set of  $\lambda$ , which impacts the topology and the features of the generator such as  $p_p$ ; the type of windings; etc. Several studies suggest different  $\lambda$  values, such as: 0.58 [51], 0.63 [52], 0.315–0.375 [43,49], 0.6–0.7 [53].

$$D_i = D_0 \cdot \lambda \quad (12)$$

To maximise the magnetic field generated by the PMs, the number of PMs ( $N_{PM}$ ) and their size (length  $l_1$ , height  $l_2$ ) are chosen by covering the maximum available rotor area ( $A_r$ ) [54], as indicated by Equations (13) and (14) [55]. The study [55] proposes an edge value not covered by PMs ( $e_r$ ) of 0.8722 for an optimal construction value. The number of stator slots ( $s_1$ ) and  $p_p$  has been chosen of equal value to  $N_{PM}$  to maximize the number of active sides of the coils and therefore the  $P_{out}$  [29].

$$A_r = \left[ \left( \frac{D_0}{2} - e_r \right)^2 - \left( \frac{D_i}{2} - e_r \right)^2 \right] \frac{\pi}{2} \quad (13)$$

$$N_{PM} = \frac{A_r}{l_1 \cdot l_2} \quad (14)$$

The typology and the characteristics of the windings (such as the layout, the number of layers, the peripheral development of the coils, the design of the coil heads; the connection between the coils, etc.) are identified by the parameters defined by Equations (15)–(17) [29,56], such as the number of coils per phase ( $n_c$ ); the number of slots per pole per phase ( $q_1$ ) and the electrical angle between the slots of the same phase ( $\gamma$ ).

$$n_c = \frac{s_1}{2m_1} \quad (15)$$

$$q_1 = \frac{s_1}{p_p m_1} \quad (16)$$

$$\gamma = \frac{360}{s_1} p_p \quad (17)$$

The pole pitch ( $\tau_p$ ) indicates the distance between the slots containing the active sides of a coil, the tooth pitch ( $\tau_c$ ) indicates the distance between the slots. These parameters are shown in Equations (18) and (19) [53], according to the average radius of the generator ( $R_m$ ).

$$\tau_p = \frac{2\pi R_m}{p_p} \quad (18)$$

$$\tau_c = \frac{2\pi R_m}{(s_1/p_p)} \quad (19)$$

The optimal winding number of turns can be calculated by Equation (20) [29] through the stator current ( $I_a$ ) and the current density ( $A_m$ ).

$$N = \frac{\pi D_0 (1 + \lambda) A_m}{4 m_1 \sqrt{2} I_a} \quad (20)$$

Once the number of coils is determined, it is possible to find the maximum cross-section of the conductor of which the winding is formed ( $S_w$ ) by the size of the slot cross-section ( $S_c$ ); the number of winding layers ( $n_s$ ) and the slot fill factor ( $f_c$ ) [57] as shown in Equation (21) [46].

$$S_w = \frac{S_c f_c}{N n_s} \quad (21)$$

### 3. Parametrical Study of Three-Phase and Single-Phase Axial Flux Permanent Magnet Synchronous Generators for Pico Hydropower Application

A parametrical study of three-phase and single-phase Axial Flux Permanent Magnet Synchronous Generators for pico hydropower application was developed to determine the performance achievable by miniaturising an AFPMGS.

Three different construction topologies of the generator, views and with a cross-section of the rotor to display the internal structure are shown in Figure 3a–c, were considered:

- $M_1$  is a three-phase AFPMGS with 2 polar pairs and single-layer concentrated windings;
- $M_2$  is a single-phase AFPMGS with 4 polar pairs and double-layer concentrated windings;
- $M_3$  is a single-phase AFPMGS with 3 polar pairs and double-layer concentrated windings.

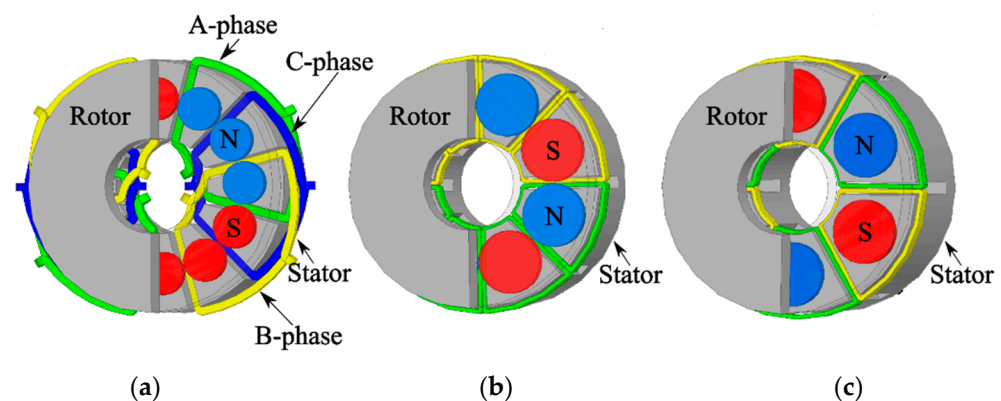


**Figure 3.**  $M_1$  (a);  $M_2$  (b);  $M_3$  (c) topologies representation with a cross-section of the rotor, magnets and coils.

Each topology has a single slotted stator and a single rotor with an outer diameter of 71 mm and a rotor height of 9.4 mm. The three configurations were realized with surface-mounted PMs to facilitate its building process. The whole structure of the AFPMGS used in this study has been designed considering cost effective choices. In fact, the diameters ( $D_{PM}$ ) of the 3 mm thick cylindrical PMs have been selected among those commercially

available in order to allow the production a low-cost machine. The PMs of Neodymium Iron Boron earth magnets (NdFeB) with  $H_c$  of 860–995 kA/m and  $B_r$  of 1.32–1.39 T were used, due to their availability on the market at an affordable cost.

The concentrated windings were commonly used in small power generators [56] as they are simple-to-build [58], and lower joule losses [59]. In Single-layer concentrated winding used in  $M_1$  topology, each side of the coil fully occupies the stator slot as shown in Figure 4a; in double-layer concentrated winding used in  $M_2$  and  $M_3$  topologies, two coils are overlapped, each one occupying only half of the stator slot as shown in Figure 4b,c.

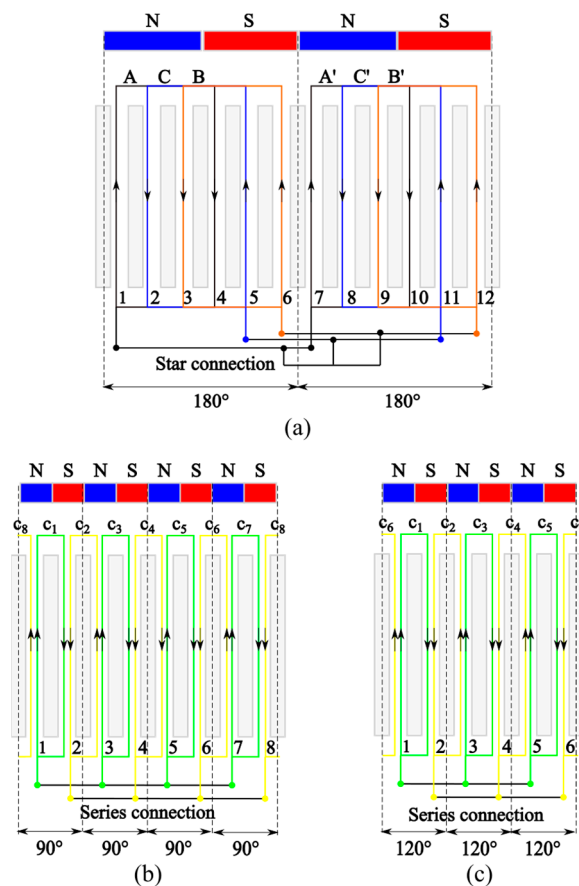


Figure 4. Winding layout of topologies  $M_1$  (a),  $M_2$  (b),  $M_3$  (c).

The windings of the  $M_1$  three-phase topology were realised with phases A, B, C arranged with 120 degrees phase shift each other; while the single-phase  $M_2$  and  $M_3$  topologies were realised with coils offset by 90 degrees to each other. Table 2 displays the winding arrangement details: the first slot number identifies the forward coil slot, and the second one the return coil slot. The coils  $A_1, B_1, C_1$  and  $A'_1, B'_1, C'_1$  of the  $M_1$  topology was star connected; while the coils  $c_1, c_3, c_5, c_7$  and  $c_2, c_4, c_6, c_8$  of topology  $M_2$  were connected in series, and the two coils group were connected in parallel. The same occurs for coils  $c_1, c_3, c_5$  and  $c_2, c_4, c_6$  of topology  $M_3$ .

Table 2. Winding arrangement details.

$M_1$	coil slot	$A_1$ 1-4	$B_1$ 6-3	$C_1$ 5-2	$A'_1$ 7-10	$B'_1$ 12-9	$C'_1$ 11-8		
$M_2$	coil slot	$c_1$ 1-2	$c_2$ 3-2	$c_3$ 3-4	$c_4$ 4-5	$c_5$ 5-6	$c_6$ 7-6	$c_7$ 7-8	$c_8$ 1-8
$M_3$	coil slot	$c_1$ 1-2	$c_2$ 3-2	$c_3$ 3-4	$c_4$ 5-4	$c_5$ 5-6	$c_6$ 1-6		

The PM and winding phase configuration in the proposed topologies allows a design symmetry of 180 degrees for the  $M_1$  topology, 90 degrees for  $M_2$  topology, and 120 degrees for the  $M_3$  topology.

A copper conductor resin insulated with a cross-section of 0.8 and 1.4 is used for the windings of the three-phase topology and single-phase topologies, respectively. The cross-section of the conductor was sized to obtaining a current density value of 2 A/mm<sup>2</sup>.

The number of turns of the coil was set to maintain the peak voltage value induced on the windings lower than the 25 V (safety voltage threshold). This allows the design of a generator intrinsically safe against electrocution thanks to the use of the very low safety voltage and which can be employed in different applications without the requirement of additional safety systems. The construction features of the proposed topologies are shown in Table 3.

**Table 3.** Topologies  $M_1$ ,  $M_2$  and  $M_3$  features.

Topology Name	$M_1$	$M_2$	$M_3$
Type of phases	three-phase	single-phase	single-phase
Number of slots	12	8	6
Number of polar pairs	2	4	3
Pole pitch	3	1	1
Number of winding layers	single-layer	double-layer	double-layer
Cross-section of the winding conductor (mm <sup>2</sup> )	0.8	1.4	1.4
Number of coils	6	8	6
Number of coils in series per phase	2	4	3
Outer diameter (mm)	71	71	71
Slot height (mm)	16	24.4	32.2
Slot width (mm)	5.3	8.0	10.7
Stator length (mm)	25.5	33.5	41.6
Rotor length (mm)	9.4	9.4	9.4

For each of the proposed topologies, the following construction parameters were considered:

- the slot fill factor,  $f_r$ , assumed 0.7 for the easy manufacture of the windings and 1 to maximize the induced voltage on the coils and the magnetic flux produced;
- the ratio between internal and outer diameter,  $\lambda$  of value 0.37, 0.58, 0.63, 0.70 typical values for industrial use [43,49,51–53];
- the thickness of the air-gap,  $g$  of 0.5 and 1 mm values used in industry [48] that limit the increase in air-gap reluctance and considers the manufacturing difficulties of a small machine increasing the ease of assembly and maintenance.

The impact of these parameters on  $P_{out}$  was evaluated in 16 different configurations of each proposed topology as summarized in Table 4. The main constructive parameters are shown in Figure 5, which indicates the definition of some parameters listed in the previous table.

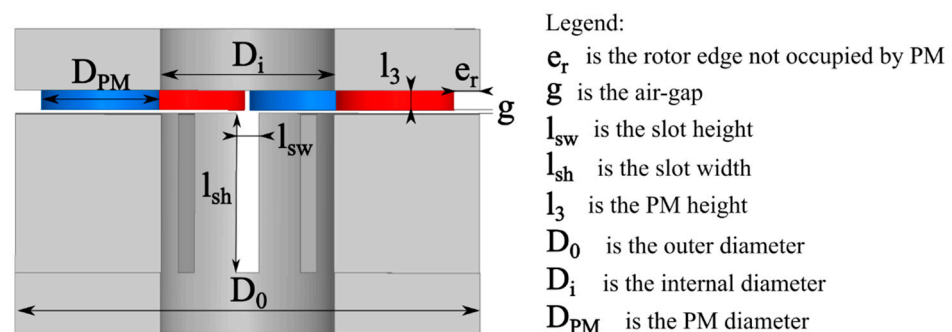


**Figure 5.** AFPMSG geometry and main parameters.



**Table 4.** AFPMGS configurations.

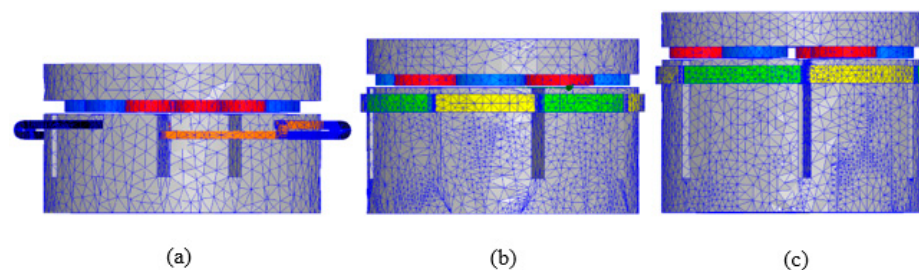
Configuration Name	$D_{PM}$ (mm)	$e_r$ (mm)	$\lambda$	$D_i$ (mm)	$N$	$f_r$	$g$ (mm)
1	14	0.45	0.58	41.2	200/220/390	1	1
2					0.5		
3					1		
4					0.5		
5	12	0.56	0.63	44.7	200/220/390	1	1
6					0.5		
7					1		
8					0.5		
9	18	2.10	0.37	26.6	200/220/390	1	1
10					0.5		
11					1		
12					0.5		
13	10	0.32	0.70	49.7	200/220/390	1	1
14					0.5		
15					1		
16					0.5		

All AFPMSG topology and configurations were developed with a 3-D modelling and Finite Element Analysis (FEA) [60] in Ansoft Maxwell software, with the aim of evaluating the effects of different construction parameters on the output power. The performances achieved through no-load and load tests were evaluated with the following values:

- the voltage magnitude induced in the stator winding;
- the magnetic field value in the parts of the proposed generators.

To execute the load test, the  $M_1$  three-phase generators were supplied with a current of 1.6 A, the  $M_2$  and  $M_3$  single-phase with a current of 2.4 A according to the cross-section of the windings conductor.

The FEA was developed splitting the AFPMGS into different mesh sizes tetrahedra [61]. To evaluate the variables of interest in specific geometric details such as non-symmetrical structures and corners, the tetrahedra dimension was smaller into the structure and bigger in the air-gap [62]. Considering the small size of the generator, the mesh decomposition used is set of 12,000, 14,000, 18,000 elements in the windings and of 40,000, 50,000, 60,000 elements in the stator and rotor, for  $M_1$ ,  $M_2$ , and  $M_3$  topologies respectively. For each topology, the representation of the tetrahedron division of the 3-D topologies is shown in Figure 6.

**Figure 6.** 3-D representation of mesh decomposition for  $M_1$  (a);  $M_2$  (b) and  $M_3$  (c) topologies.

#### 4. Results and Discussions

The parametrical study performed on the topologies and configurations of the proposed AFPMGS has allowed to evaluate the magneto dynamic behavior as well as its achievable performances. The authors have performed more than 100 simulations evaluating the power output, the induced voltage in the stator windings and the magnetic field under an operating condition of 1000 rpm of rotor angular speed. Also, the performance

and the magneto dynamic behavior of the highest power output AFPMGS under a 100 to 1000 rpm operating condition was investigated.

#### 4.1. Assessment and Comparison of the Performance of the Proposed Topologies

By evaluating the peak-to-peak voltage magnitude ( $V_p$ ) induced in one phase of the stator winding and the peak-to-peak magnitude of flux density in air-gap ( $B_p$ ) the 48 proposed configurations were tested in no-load and load condition with a speed of 1000 rpm. The results of the tests are compared in Figures 7 and 8. Topologies  $M_2$  and  $M_3$  shown similar voltage magnitude trends for the various configurations, with a higher value for 9, 10, and 12 configurations. For these configurations, the topology  $M_3$  presents a higher  $V_p$  value due to the use of a higher number of turns. The magnitude flux density in air-gap in  $M_1$  configurations using 18 mm and 14 mm diameter magnets are higher. The magnitude flux density in the air-gap of configurations with  $g$  of 1 mm presents a lower value than configurations with  $g$  of 0.5 mm.

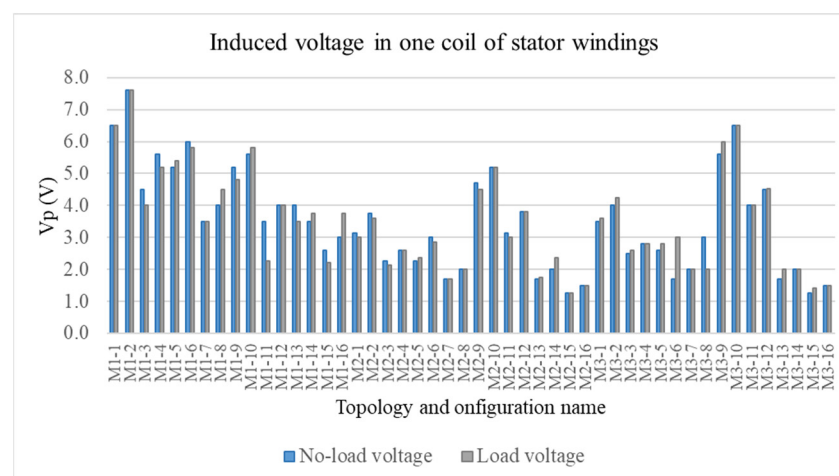


**Figure 7.** The induced voltage of one phase in the no-load and load tests for different configurations.

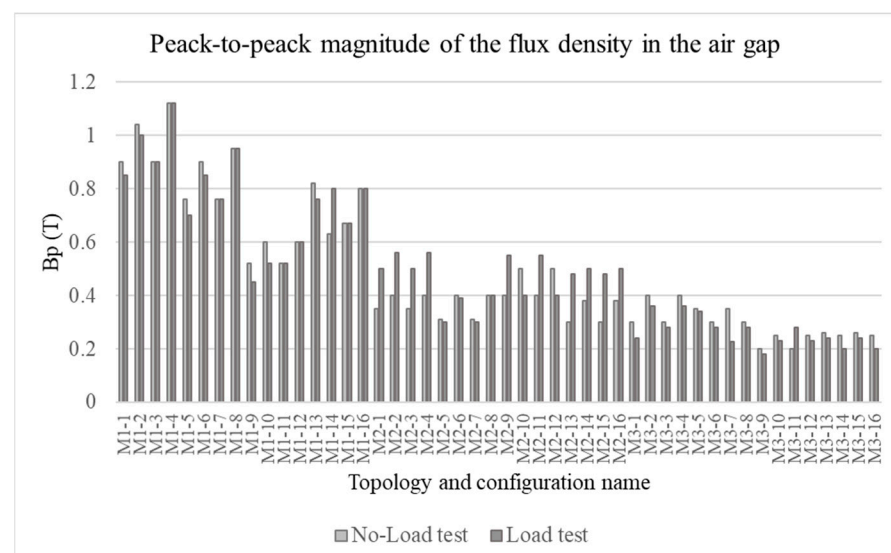


**Figure 8.** The flux density in air-gap for no-load and load tests of different configurations.

The AFPMGS performances were compared determining the power output of each configuration according to Equation (11), taking into account the connections between the coils. As shown in Figure 9, the highest values of  $P_{out}$  were reached by the  $M_2$  topology realised with configuration 10, which allows to obtain an output power of 70.5 W.

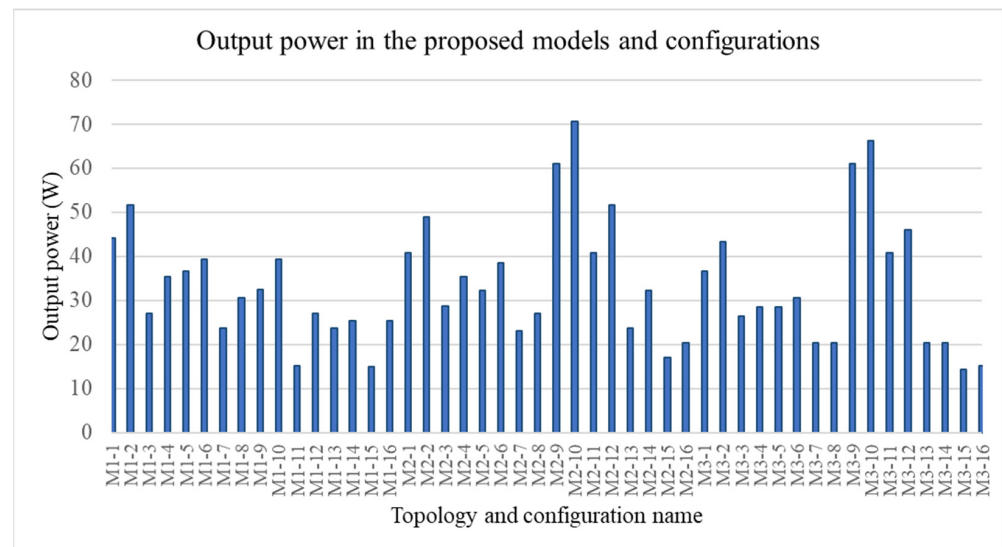


**Figure 9.** The output power of different topologies and configurations.

#### 4.2. Analysis of the Highest Performance Topology under Different Working Conditions

The 10 configurations of  $M_2$  model were designed with a N-S layout of the PMs, which provides a balanced flux path within the AFPMGS core. The magnetic flux density vector path is shown in Figure 10. The magnetic flux density generated during the working conditions of the AFPMGS is higher inside the coil and assumes values of 0.5–1.23 T without saturating any component; besides part of the flux is leakage on the external surfaces of the stator and rotor and assumes values of about 0.2–0.5 T.

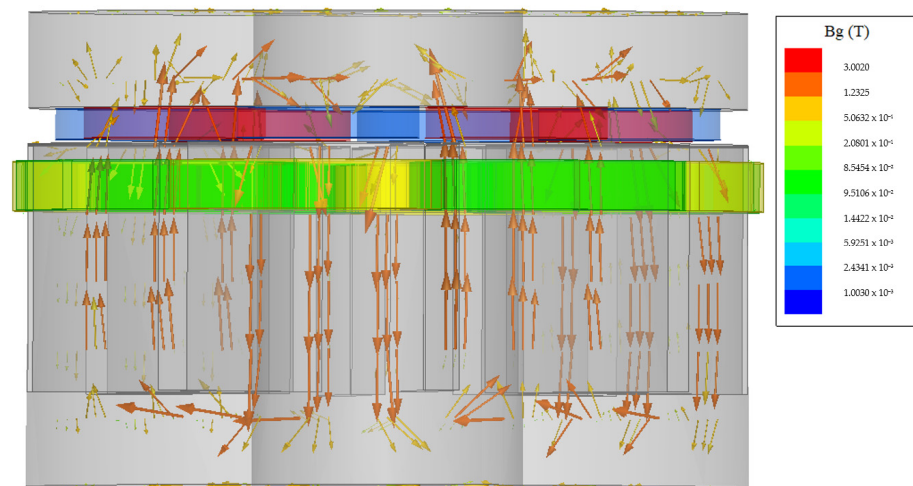
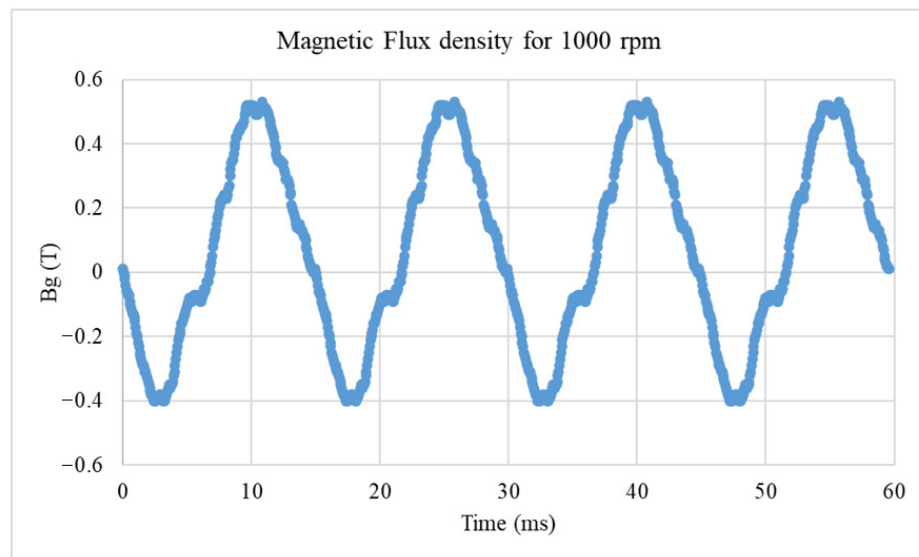
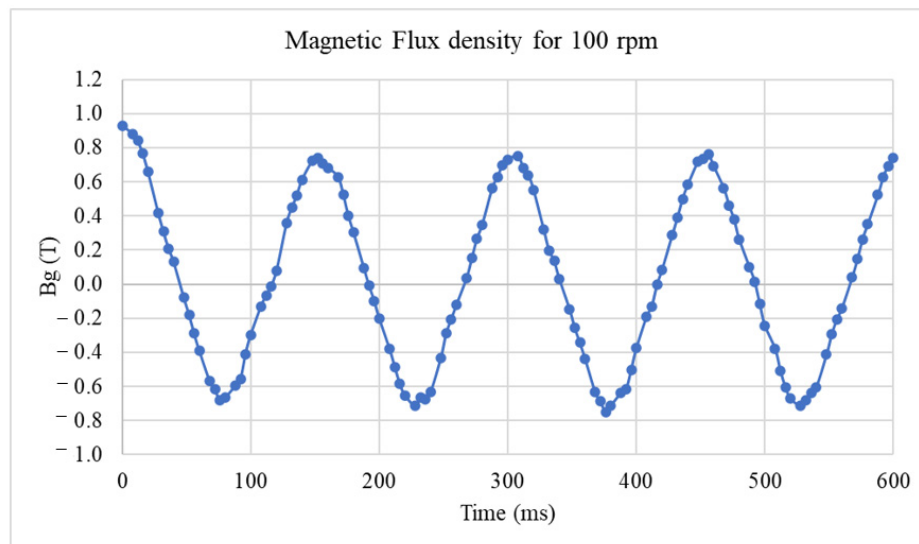


**Figure 10.** Magnetic flux density vector path of  $M_2$  with configuration 10.

To simulate the performance of the proposed AFPMGS coupled with a turbine under different operating conditions, the magneto dynamic behavior of the configuration 10 of  $M_2$  topology was evaluated by carrying out tests under load, varying the rotor speed from 100 to 1000 rpm with a 100 rpm step. Figure 11 shows the magnetic field trend at the air gap during a rotation at 100 and 1000 rpm. The waveform achieved using 1000 rpm is close to a sinusoidal trend due to the design and configuration settings for the generator, that allow to reduce the distortion caused by circular PMs placed too close together. Harmonics of the Magnetic flux density trend at 100 rpm waveform were identified using the Fast Fourier Transform (FFT), as shown in Figure 12.



(a)



(b)

Figure 11. Magnetic flux density trend at 1000 rpm (a) and 100 rpm (b) of  $M_2$  with configuration 10.

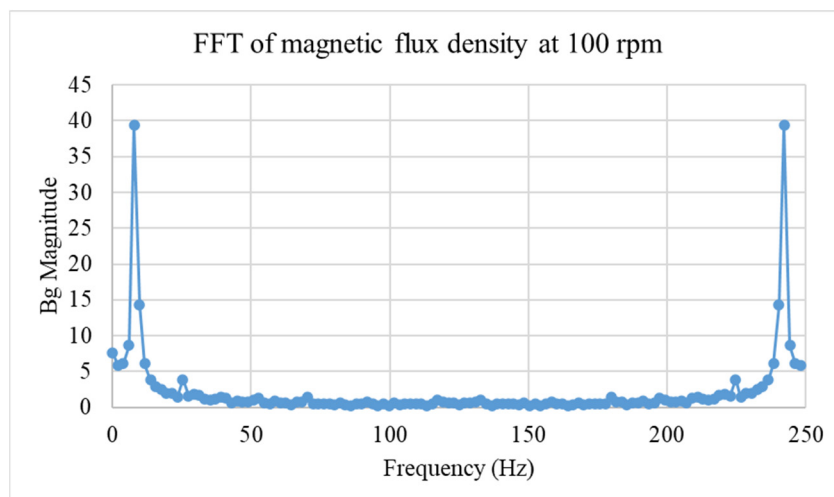


Figure 12. FFT of magnetic flux density trend at 100 rpm.

The magnitude flux density in the air-gap obtained for the speeds between 100 and 1000 rpm has decreased from 0.8 to 0.44 T. This decrease is linear in the speed range of 100–500 rpm. In conclusion, using the configuration 10 of  $M_2$  topology a power output of 29.7 W at 100 rpm and a maximum power of 70.5 W at 1000 rpm was achieved.

## 5. Conclusions

Pico hydropower applications allow the harvesting of energy using the power of the water flowing in small watercourses, water waste treatment plants, and water distribution network. The miniaturisation of this technology realised with AFPMGs, allows to generate high power values with small dimensions and to supply small domestic loads enables the electrification of rural areas in a cost-effective manner. The authors proposed a parametrical study of several configurations and topologies of extra low-voltage AFPMGs. The parametrical study was performed by evaluating 3 different topologies ( $M_1$ ;  $M_2$ ;  $M_3$ ), one single-phase and two three-phases, realized with one stator and rotor, commercial NdFeB PMs, concentric winding with 1 or 2 layers. The  $P_{out}$  of these topologies was evaluated in 48 different configurations, obtained by varying the constructive parameter as  $\lambda$ ,  $f_c$ , and  $g$ , through the 3-D modellization performed on the Ansoft Maxwell software and the use of FEA analysis. This analysis allows to evaluate the output voltage trends and the flux density distribution on each component of the generator, including the air-gap.

Among the different configurations, the  $P_{out}$  highest values, for a generator of  $0.687 \text{ cm}^3$ , were equal to 70.5 W at 1000 rpm and equal to 29.7 W at 100 rpm, corresponding respectively to 1.7 kWh/day and 0.71 kWh/day in continuous working. These  $P_{out}$  values were obtained for the configuration 10 of the single-phase  $M_2$  topology, ( $D_0 = 71 \text{ mm}$ ,  $g = 0.5 \text{ mm}$ ,  $\lambda = 0.375$ , 8 surface-mounted PM,  $D_{PM} = 18 \text{ mm}$ , double-layer concentric winding with 8 coils,  $N = 200$  and  $f_c = 1$ ).

The pico-hydropower system here investigated, due to the AFPMGs small size, can be installed in water pipelines to supply household loads or storage batteries, supporting the on-site production of electricity from renewable sources. In further studies the application of pico-hydropower plants installed in the urban water system as water distribution network will be considered, with the aim to investigate the capacity of these systems to feed high load values, supporting the decarbonisation and increasing the distributed generation.

**Author Contributions:** Conceptualization, methodology, supervision of simulations and contributed to all draft: G.C., D.M. and V.D.D.; software implementation, writing original draft preparation, writing review and editing G.C. and D.M. The contribution of the authors equally shared. All authors have read and agreed to the published version of the manuscript.

**Funding:** This research received no external funding.

**Acknowledgments:** The authors are thankful to the company AMAP. S.p.A., who supported this research.

**Conflicts of Interest:** The authors declare no conflict of interest.

## Nomenclature

$A$	total electrical load (W);
$A_m$	current density ( $\text{A}/\text{mm}^2$ );
$A_r$	rotor surface ( $\text{mm}^2$ );
$B_g$	flux density in air-gap (T);
$B_p$	peak-to-peak magnitude of flux density in air-gap;
$B_r$	remanence (T);
$D_0$	outer diameter of the generators (mm);
$D_i$	internal diameter of the generators (mm);
$D_{PM}$	diameter of PM (mm);
$e(t)$	phase air-gap EMF (V);
$e_r$	rotor edge not occupied by PM (mm);

$E_{pk}$	peak of phase air-gap EMF (V);
$f$	frequency of the inverter (Hz);
$f_c$	slot fill factor;
$g$	thickness of the air-gap (mm);
$H_c$	coercive field of the PM (kA/m);
$I_a$	stator current (A);
$i(t)$	phase current (A);
$I_{pk}$	peak of current (A);
$I_{sh}$	slot height (mm);
$I_{sw}$	slot width (mm);
$K_e$	EMF factor;
$K_i$	current waveform factor;
$K_L$	aspect ratio coefficient of the type of machines;
$K_p$	electrical power waveform factor;
$K_\phi$	electrical loading ratio on the rotor and stator;
$l_1$	height of the PM (mm);
$l_2$	width of the PM (mm);
$l_3$	thickness of the PM (mm);
$L_e$	axial length of the generator (mm);
$m$	number of phases;
$m_1$	number of phases of each stator;
$N$	winding number of turns;
$n_c$	number of coils per phase;
$N_{ph}$	number of winding turns per phase;
$N_{PM}$	number of PM;
$n_s$	number of layers of the winding;
$p_p$	number of polar pairs;
$P_{out}$	power output (W);
$q_1$	number of slots per pole and per phase;
$R_m$	average radius of the generator (mm);
$s_1$	number of slots;
$S_c$	cross-section of the slot (mm <sup>2</sup> );
$S_w$	maximum conductor cross-section (mm <sup>2</sup> );
$T$	period of one EMF cycle (s);
$V_p$	peak-to-peak magnitude voltage induced in one phase of the stator winding.
<i>Greek Alphabet</i>	
$\eta$	generator efficiency;
$\lambda$	ratio between the internal and outer diameter;
$\gamma$	electrical angle between the slots of the same phase (°);
$\tau_p$	pole pitch;
$\tau_c$	tooth pitch;
$\mu_0$	vacuum permeability (H/m).
<i>Abbreviations</i>	
3-D	three dimensional;
AC	alternate current;
AFPMGS	axial flux permanent magnet synchronous generator;
NdFeB	neodymium iron boron earth magnets;
DC	direct current;
FEA	finite element analysis;
IG	Induction Generators;
PM	permanent magnet;
PMSG	permanent magnet synchronous generator;
Rpm	rotation per minutes;
SG	synchronous generator;
FFT	Fast Fourier Transform.

## References

1. Balkhair, K.S.; Rahman, K.U. Sustainable and economical small-scale and low-head hydropower generation: A promising alternative potential solution for energy generation at local and regional scale. *Appl. Energy* **2017**, *188*, 378–391. [[CrossRef](#)]
2. Liu, H.; Brown, T.; Andresen, G.B.; Schlachtberger, D.P.; Greiner, M. The role of hydro power, storage and transmission in the decarbonization of the Chinese power system. *Appl. Energy* **2019**, *239*, 1308–1321. [[CrossRef](#)]
3. Qin, P.; Xu, H.; Liu, M.; Xiao, C.; Forrest, K.E.; Samuelsen, S.; Tarroja, B. Assessing concurrent effects of climate change on hydropower supply, electricity demand, and greenhouse gas emissions in the Upper Yangtze River Basin of China. *Appl. Energy* **2020**, *279*, 115694. [[CrossRef](#)]
4. Basso, S.; Lazzaro, G.; Bovo, M.; Soulsby, C.; Botter, G. Water-energy-ecosystem nexus in small run-of-river hydropower: Optimal design and policy. *Appl. Energy* **2020**, *280*, 115936. [[CrossRef](#)]
5. Patro, E.R.; De Michele, C.; Avanzi, F. Future perspectives of run-of-the-river hydropower and the impact of glaciers' shrinkage: The case of Italian Alps. *Appl. Energy* **2018**, *231*, 699–713. [[CrossRef](#)]
6. Gaudard, L.; Avanzi, F.; De Michele, C. Seasonal aspects of the energy-water nexus: The case of a run-of-the-river hydropower plant. *Appl. Energy* **2018**, *210*, 604–612. [[CrossRef](#)]
7. International Hydropower Association (IHA). *Hydropower Status Report 2020*; International Hydropower Association (IHA): London, UK, 2020.
8. International Hydropower Association (IHA). *Hydropower Status Report 2015*; International Hydropower Association (IHA): London, UK, 2015.
9. Rapporto Statistico. *Energia da Fonti Rinnovabili in Italia*; Technical Report; Rapporto Statistico: Rome, Italy, 2015.
10. Rapporto Statistico. *Energia da Fonti Rinnovabili in Italia*; Technical Report; Rapporto Statistico: Rome, Italy, 2018.
11. Kuriqi, A.; Pinheiro, A.N.; Sordo-Ward, A.; Garrote, L. Flow regime aspects in determining environmental flows and maximising energy production at run-of-river hydropower plants. *Appl. Energy* **2019**, *256*, 113980. [[CrossRef](#)]
12. Singh, P.; Nestmann, F. Experimental optimization of a free vortex propeller runner for micro hydro application. *Exp. Therm. Fluid Sci.* **2009**, *33*, 991–1002. [[CrossRef](#)]
13. Carravetta, A.; Fecarotta, O.; Sinagra, M.; Tucciarelli, T. Cost-benefit analysis for hydropower production in water distribution networks by a pump as turbine. *J. Water Resour. Plan. Manag.* **2014**, *140*, 04014002. [[CrossRef](#)]
14. Tarroja, B.; Forrest, K.; Chiang, F.; AghaKouchak, A.; Samuelsen, S. Implications of hydropower variability from climate change for a future, highly-renewable electric grid in California. *Appl. Energy* **2019**, *237*, 353–366. [[CrossRef](#)]
15. Khomsah, A.; Sudjito; Wijono; Laksono, A.S. Pico-hydro as A Renewable Energy: Local Natural Resources and Equipment Availability in Efforts to Generate Electricity. In *IOP Conference Series: Materials Science and Engineering*; IOP Publishing Ltd.: Bristol, UK, 2019; Volume 462, p. 012047.
16. AMusyafiq, A.A.; Ilahi, N.A.; Dewi, R.P.; Barokah, U. Simulation of Piko Hydro Power Generator Using Thread Turbine With 10 Watt Power. *J. Jartel J. Jar. Telekomun.* **2022**, *12*, 100–104.
17. Venkatesh, P.; Viswanadha, V.; Sravan Kumar, K.; Ramesh, K. Design of Pico Hydro Power Plant Using an Impulse Turbine. In *Advanced Manufacturing Systems and Innovative Product Design*; Springer: Berlin/Heidelberg, Germany, 2021; pp. 251–260.
18. Wahab, M.H.A.; Ching, K.B. Pico Hydro Generator Module for Domestic Water Pipe Fitting. *Evol. Electr. Electron. Eng.* **2022**, *3*, 321–331.
19. Williams, A.; Simpson, R. Pico hydro—Reducing technical risks for rural electrification. *Renew. Energy* **2009**, *34*, 1986–1991. [[CrossRef](#)]
20. Taylor, S.D.; Fuentes, M.; Green, J.; Rai, K. *Stimulating the Market for Pico-Hydro in Ecuador*; IT Power: Bristol, UK, 2003.
21. Ming, B.; Liu, P.; Guo, S.; Zhang, X.; Feng, M.; Wang, X. Optimizing utility-scale photovoltaic power generation for integration into a hydropower reservoir by incorporating long- and short-term operational decisions. *Appl. Energy* **2017**, *204*, 432–445. [[CrossRef](#)]
22. Maher, P.; Smith, N.; Williams, A. Assessment of pico hydro as an option for off-grid electrification in Kenya. *Renew. Energy* **2003**, *28*, 1357–1369. [[CrossRef](#)]
23. Boukhezzar, B.; Siguerdidjane, H. Nonlinear control with wind estimation of a DFIG variable speed wind turbine for power capture optimization. *Energy Convers. Manag.* **2009**, *50*, 885–892. [[CrossRef](#)]
24. Sarasúa, J.I.; Pérez-Díaz, J.I.; Wilhelmi, J.R.; Sánchez-Fernández, J.Á. Dynamic response and governor tuning of a long penstock pumped-storage hydropower plant equipped with a pump-turbine and a doubly fed induction generator. *Energy Convers. Manag.* **2015**, *106*, 151–164. [[CrossRef](#)]
25. Naeini, V.; Ardebili, M. New axial flux PM less synchronous machine with concentrated DC field on stator. *Int. J. Electr. Power Energy Syst.* **2015**, *67*, 651–658. [[CrossRef](#)]
26. Paul, S.; Chang, J. Model-based design of variable speed non-salient pole permanent magnet synchronous generator for urban water pipeline energy harvester. *Int. J. Electr. Power Energy Syst.* **2021**, *125*, 106402. [[CrossRef](#)]
27. Barcaro, M.; Bianchi, N. Interior PM Machines Using Ferrite to Replace Rare-Earth Surface PM Machines. *IEEE Trans. Ind. Appl.* **2014**, *50*, 979–985. [[CrossRef](#)]
28. Widyan, M.S.; Hanitsch, R.E. High-power density radial-flux permanent-magnet sinusoidal three-phase three-slot four-pole electrical generator. *Int. J. Electr. Power Energy Syst.* **2012**, *43*, 1221–1227. [[CrossRef](#)]

29. Gieras, J.F.; Wang, R.-J.; Kamper, M.J. *Axial Flux Permanent Magnet Brushless Machines*, 2nd ed.; Springer Netherlands: Dordrecht, The Netherlands, 2008; pp. 1–362.
30. Kurt, E.; Gör, H.; Demirtaş, M. Theoretical and experimental analyses of a single phase permanent magnet generator (PMG) with multiple cores having axial and radial directed fluxes. *Energy Convers. Manag.* **2014**, *77*, 163–172. [[CrossRef](#)]
31. Flores, E.; Cumbajin, M.; Sanchez, P. Design of a synchronous generator of permanent magnets of radial flux for a pico-hydropower station. In *Advances and Applications in Computer Science, Electronics and Industrial Engineering*; Springer: Berlin/Heidelberg, Germany, 2021; pp. 135–151.
32. Róowicz, S.; Goryca, Z.; Peczkis, G.; Korczak, A. Pico hydro generator as an effective source of renewable energy. *Przełkad Elektrotechniczny* **2019**, *4*, 200–204. [[CrossRef](#)]
33. Wannakarn, P.; Tanmaneeprasert, T.; Rugthaicharoencheep, N.; Nedphograw, S. Design and construction of axial flux permanent magnet generator for wind turbine generated DC voltage at rated power 1500 W. In Proceedings of the 2011 4th International Conference on Electric Utility Deregulation and Restructuring and Power Technologies (DRPT), Weihai, China, 6–9 July 2011; pp. 763–766.
34. Safdar, I.; Sultan, S.; Raza, H.A.; Umer, M.; Ali, M. Empirical analysis of turbine and generator efficiency of a pico hydro system. *Sustain. Energy Technol. Assess.* **2020**, *37*, 100605. [[CrossRef](#)]
35. Zainuddin, H.; Yahaya, M.S.; Lazi, J.M.; Basar, M.F.M.; Ibrahim, Z. Design and development of pico-hydro generation system for energy storage using consuming water distributed to houses. *World Acad. Sci. Eng. Technol.* **2009**, *59*, 154–159.
36. Smith, N.P.A. Induction Generators for Stand-Alone Micro-Hydro Systems. In Proceedings of the IEEE International Conference on Power Electronics, Drives & Energy Systems for Industrial Growth (PEDES), New Delhi, India, 8–11 January 1996; Volume 2, pp. 669–673.
37. Bozorgi, A.; Javidpour, E.; Riasi, A.; Nourbakhsh, A. Numerical and experimental study of using axial pump as turbine in Pico hydropower plants. *Renew. Energy* **2013**, *53*, 258–264. [[CrossRef](#)]
38. Green, J.; Fuentes, M.; Rai, K.; Taylor, S. *Stimulating the picohydropower market for low-income households in Ecuador*; The World Bank: Washington, DC, USA, 2005.
39. Chan, T.F.; Lai, L.L. An Axial-Flux Permanent-Magnet Synchronous Generator for a Direct-Coupled Wind-Turbine System. *IEEE Trans. Energy Convers.* **2007**, *22*, 86–94. [[CrossRef](#)]
40. Kahourzade, S.; Mahmoudi, A.; Ping, H.W.; Uddin, M.N. A Comprehensive Review of Axial-Flux Permanent-Magnet Machines. *Can. J. Electr. Comput. Eng.* **2014**, *37*, 19–33. [[CrossRef](#)]
41. Caricchi, F.; Crescimbin, F.; Honorati, O.; Bianco, G.L.; Santini, E. Performance of coreless-winding axial-flux permanent-magnet generator with power output at. *IEEE Trans. Ind. Appl.* **1998**, *34*, 1263–1269. [[CrossRef](#)]
42. Laxminarayan, S.S.; Singh, M.; Saifee, A.H.; Mittal, A. Design, modeling and simulation of variable speed Axial Flux Permanent Magnet Wind Generator. *Sustain. Energy Technol. Assess.* **2017**, *19*, 114–124. [[CrossRef](#)]
43. Huang, S.; Luo, J.; Leonardi, F.; Lipo, T. A comparison of power density for axial flux machines based on general purpose sizing equations. *IEEE Trans. Energy Convers.* **1999**, *14*, 185–192. [[CrossRef](#)]
44. Kahourzade, S.; Mahmoudi, A.; Gandomkar, A.; Abd Rahim, N.; Ping, H.W.; Uddin, M.N. Design optimization and analysis of AFPM synchronous machine incorporating power density, thermal analysis, and back-EMF THD. *Prog. Electromagn. Res.* **2013**, *136*, 327–367. [[CrossRef](#)]
45. Leong, Y.W.; Razali, A.R.; Priyandoko, G.; Kasim, N.I. Preliminary Studies on Number of Coil Turns per Phase and Distance between the Magnet Pairs for AFPM Ironless Electricity Generator. *MATEC Web Conf.* **2016**, *38*, 03003. [[CrossRef](#)]
46. Kostenko, M.; Piotrovskii, L. *Electric Machines*; Energiia: Leningrad, Russia, 1969.
47. Huang, S.; Luo, J.; Leonardi, F.; Lipo, T. A general approach to sizing and power density equations for comparison of electrical machines. *IEEE Trans. Ind. Appl.* **1998**, *34*, 92–97. [[CrossRef](#)]
48. Saavedra, H.; Romeral, L.; Riba, J.-R. Optimal Design of a Three-Phase AFPM for In-Wheel Electrical Traction. In Proceedings of the 2014 IEEE International Electric Vehicle Conference (IEVC), Florence, Italy, 17–19 December 2014.
49. Huang, S.; Xie, G. Optimization of power density for axial-flux machine through generalized sizing equations. *J. Shanghai Univ.* **1997**, *1*, 232–236. (In English) [[CrossRef](#)]
50. Puri, V.; Chauhan, Y.K.; Singh, N. A comparative design study and analysis of inner and outer rotor permanent magnet synchronous machine for power generation in vertical axis wind turbine using GSA and GSA-PSO. *Sustain. Energy Technol. Assess.* **2017**, *23*, 136–148. [[CrossRef](#)]
51. Campbell, P. Principles of a Permanent-Magnet Axial-Field Dc Machine. *Proc. Inst. Electr. Eng.* **1974**, *121*, 1489–1494. [[CrossRef](#)]
52. Caricchi, F.; Crescimbin, F.; Fedeli, E.; Noia, G. Design and construction of a wheel-directly-coupled axial-flux PM motor prototype for EVs. In Proceedings of the 1994 IEEE Industry Applications Society Annual Meeting, Denver, CO, USA, 2–6 October 1994; Volume 1, pp. 254–261.
53. Jokinen, T.; Hrabovcova, V.; Pyrhonen, J. *Design of Rotating Electrical Machines*; John Wiley & Sons: Hoboken, NJ, USA, 2013.
54. Meier, F.; Soulard, J. PMSMs with non-overlapping concentrated windings: Design guidelines and model references. *Ecol. Veh. Renew. Energy. (EVER 09)* **2009**, 26–29.
55. Cetin, E.; Daldaban, F. Analyzing the Profile Effects of the Various Magnet Shapes in Axial Flux PM Motors by Means of 3D-FEA. *Electronics* **2018**, *7*, 13. [[CrossRef](#)]
56. Yahaya, E.A. Single layer winding of three phase induction motor. *Int. J. Eng. Sci.* **2013**, *2*, 8–13.



57. Libert, F.; Soulard, J. Investigation on pole-slot combinations for permanent-magnet machines with concentrated windings. In Proceedings of the 16th International Conference on Electrical Machines, Lodz, Poland, 5–8 September 2004; pp. 530–535.
58. Geng, W.; Zhang, Z. Analysis and Implementation of New Ironless Stator Axial-Flux Permanent Magnet Machine With Concentrated Nonoverlapping Windings. *IEEE Trans. Energy Convers.* **2018**, *33*, 1274–1284. [[CrossRef](#)]
59. Ferreira, A.P.; Silva, A.M.; Costa, A.F. Prototype of an axial flux permanent magnet generator for wind energy systems applications. In Proceedings of the 2007 European Conference on Power Electronics and Applications (EPE), Aalborg, Denmark, 2–5 September 2007.
60. Musolino, A.; Raugi, M.; Rizzo, R.; Tucci, M. Optimal Design of EMALS Based on a Double-Sided Tubular Linear Induction Motor. *IEEE Trans. Plasma Sci.* **2015**, *43*, 1326–1331. [[CrossRef](#)]
61. Cipriani, G.; Corpora, M.; Di Dio, V.; Musolino, A.; Rizzo, R.; Sani, L. A comparison among different kinds of stator lamination in tubular linear machines. *Prog. Electromagn. Res. M* **2016**, *50*, 95–104. [[CrossRef](#)]
62. Rizk, J.; Nagrial, M. Design of Permanent-Magnet Generators for Wind Turbines. In Proceedings of the IPEDMC 2000: 3rd International Power Electronics and Motion Control Conference, Beijing, China, 15–18 August 2000; pp. 208–212.